JOURNAL OF SPACECRAFT AND ROCKETS
Vol. 43, No. 3, May–June 2006

Interaction Potential Between Atomic Oxygen and Polymer Surfaces in Low Earth Orbit

Laiwen Chen* and Chun-Hian Lee†
Beijing University of Aeronautics and Astronautics, 100083 Beijing, China

In the present work, an interaction potential between an incident reactive particle and a material surface is constructed. The potential is formulated based on the unit bond index-quadratic exponential potential model and two adjustable factors characterizing the correlations of equilibrium-length scales and of attractive potential. In addition, the effective potential between monomers is obtained by Lifshitz's theory. The interaction of atomic oxygen with Kapton® is computed as a test case using the potential functions developed in the present paper in conjunction with the molecular dynamic model constructed by Lee and Chen (Lee, C.-H., and Chen, L. W., "Reactive Probability of Atomic Oxygen with Material Surfaces in Low Earth Orbit," *Journal of Spacecraft and Rockets,* Vol. 37, No. 2, 2000, pp. 252–256). The reactive probability computed by the present model is found to be 16.8% lower than for the STS-46 flight data, and the law of the incident angle-dependency deduced from the flight data is also confirmed by the numerical simulation. The numerical value of the accommodation factor computed in this task is 0.1368, which lies between the values of 0.1165, computed via the hard-sphere model, and 0.68, obtained from the ground test for atomic oxygen interacting with Kapton at an impingement angle of 45 deg and energy of 1.5 eV. The effects of the two adjustable factors given in the potential model are also briefly discussed.

Nomenclature

E_i	=	initial kinetic energy, eV
$\bar{E}_i$	=	initial projectile atom translational energy, eV
$\bar{E}_f$	=	scattering atom translational energy, eV
$\boldsymbol{f}_{Y_E}(t)$	=	random force, N
k_B	=	Boltzmann constant
M_g	=	mass of the N_g atoms, kg
M_s	=	mass of the inner monomers, kg
N_g	=	labeled gas atoms
N_R	=	the number of the reactive events
N_T	=	total number of trajectories
P_R	=	reaction probability
$\langle P_R \rangle$	=	average reaction probability
$P_{R-\mathrm{LEO}}$	=	reaction probability of the flight experiment
T_S	=	initial temperature of surface, K
$V(\boldsymbol{X}, \boldsymbol{Y}_I, \boldsymbol{Y}_E, \boldsymbol{Y}_F)$	=	potential energy surface for the full system, eV
V_f	=	fundamental potential between an incoming particle and a surface, eV
$\boldsymbol{X}$	=	position of the N_g atoms
$\boldsymbol{Y}_I$	=	sets of all inner monomers over all of the layers
$\boldsymbol{Y}_E$	=	sets of all edge monomers over all of the layers
$\boldsymbol{Y}_F$	=	sets of fixed monomers over all of the layers
α	=	energy accommodation coefficient
$\langle \alpha \rangle$	=	average energy accommodation coefficient
γ	=	friction coefficient, Hz
$\delta(t)$	=	Dirac function
ε_e	=	equilibrium distance factor
ε_{gs}	=	weighting factor
θ	=	specific incident angle of the incoming oxygen, deg
θ_D	=	Debye temperature, K
ξ_{Y_E}	=	vector of Gaussian random numbers
ω_D	=	Debye frequency, Hz

Received 12 September 2004; revision received 14 February 2005; accepted for publication 25 August 2005.

*Lecturer, National Laboratory for Computational Fluid Dynamics; Lwchen@163bj.com.

†Professor, National Laboratory for Computational Fluid Dynamics; Lichx@163bj.com. Member AIAA.

I. Introduction

SPACECRAFT consist of hundreds of materials, including metals, alloys, composites, polymers, glasses, semiconductors, thermal paints, and optical coatings. Flight experiments have shown that materials suffer damage to various extents from exposure to the space environment. Primary requirements for structural materials used in spacecraft are light weight and high strength. Thus, organic-based materials or carbon-based composites are widely used in spacecraft components instead of metals. However, it has been proved that oxygen atoms cause significant erosion of many materials, particularly organic-based materials. So far, the mechanisms of atomic-oxygen effects on the polymer surfaces of spacecraft have not yet been fully understood, so that the planning and design of long-duration spacecraft in low Earth orbit (LEO) are profoundly impacted. As a consequence, the development of a theoretical approach capable of providing reliable data for engineering purposes becomes essential.

The mechanisms of interaction between energetic atomic oxygen and material surfaces in the LEO environment are discovered mainly through flight experiments or ground tests, in particular for polymeric materials.[1–5] Few theoretical works deal with interaction phenomena between atomic oxygen and polymeric materials in LEO at present, due to the dynamic complexity of the interaction. The mechanisms accounting for atomic oxygen effects are currently studied based theoretically on the theory of quantum mechanics in conjunction with the molecular dynamics in Schatz's group.[6] By correlating the impact energy of the incoming oxygen atoms and the incident angles with the reaction probability, the recombination probability of the oxygen atoms, and related effects based on the flight and ground-based experimental results, Banks et al. constructed a Monte Carlo undercutting model for analyzing the erosion of the material surfaces.[7] By employing both the line-of-centers reactive scattering model and the Beckerle–Ceyer model, Koontz et al. proposed an approach for predicting the reaction rate by means of statistical average.[8] By neglecting quantum diffraction of the oxygen atoms, and by assuming that whether an atom on

a solid surface is chemically activated depends on the tangential bonds of the atom with atoms on the surface, and that the collision of the oxygen atom can only take place with one solid atom, Baird developed a one-dimensional bond orientation model.[9]

One of the difficulties in formulating a theoretical model for the interaction between atomic oxygen and the polymeric material surface has been the construction of the interaction potentials. Following the multizone idea proposed by DePristo and Metiu,[10] the present authors formulated a model based on the theory of molecular dynamics and presented a phenomenological interaction potential of an atomic oxygen with atoms on the solid surface.[11] An alternative approach for formulating the interaction potential based on the unit bond index–quadratic exponential potential (UBI-QEP) theory is proposed in the present paper. As an illustration, we also present numerical simulation results for atomic oxygen interacting with Kapton®, a typical polymer surface material widely used in spacecraft.

II. Interaction Potentials Between an Oxygen Atom and a Solid Surface

The interaction potentials between particles in the surface material and between an oxygen atom and the surface play a crucial role in determination of the interaction of an oxygen atom with material surfaces. In this paper, we primarily consider the interaction potential between incoming particles and polymeric materials that is suitable for describing the atomic oxygen colliding with polymeric materials in the LEO environment.

Lee and Chen previously proposed[11] an interaction potential between an atomic oxygen and a surface having the following form:

$$V(r) = \varepsilon_s D_e^0 \left[\exp \frac{(r_e - r)}{a} - 2\varepsilon_{gs} \exp \frac{(r_e - r)}{2a} \right] \tag{1}$$

where D_e^0 is the depth of the potential well and r_e is the equilibrium interaction distance or the collision diameter. The surface factor ε_s counts for the correction due to the effects caused by the interaction of an oxygen atom with multiparticles on the material surface, and ε_{gs} denotes the attractive potential correction factor. Both factors can only be determined empirically. Nevertheless, numerical calculations have revealed that the interaction potential given by Eq. (1) does not provide sufficiently accurate results in predicting the interaction behavior between atomic oxygen and the polymeric surface. A more sophisticated model for interaction potential is needed.

A. Chemisorption Model

Theoretical descriptions of the interaction between incoming particles and material surfaces depend strongly upon the energy with which the interaction takes place. The mass of the projectile particle and the associated momentum transfer toward the solid also serve as significant factors in choosing the theoretical model for describing the interaction effects. As pointed out by Tenner et al., from low (thermal) to high (10-keV) energy, the surface may be viewed as evolving from a flat hard wall, through first a corrugated hard surface and then a corrugated soft surface, to an arrangement of individual atoms.[12] Consequently, theories have to treat the surface, correspondingly, as a homogeneous electron density, a hard flat or corrugated wall, a set of soft cubes, and individual atoms in a lattice, respectively. Each description has its own merit, which is valid only for a specific energy range. However, in some intermediate regions, certain mixed descriptions may occur. The particle–surface interaction may not necessarily be described as a series of purely binary interactions of the incoming particle with the surface atoms, nor can it be expressed in terms of a corrugated surface potential.

The model for the interaction potential between an incident particle and a surface is traditionally established based on the "sum of pair interactions" assumption. As a consequence, it would be difficult to fully cope with various mechanisms involved in the interaction between an incoming particle and the material surface.[13] As for the many-body interaction of a projectile particle with multiparticles on a material surface, one may intuitively argue that the overall interaction potential can be represented by a "weighted sum of pair interactions" where the pair interaction potentials can be considered as the fundamental potentials. Each of the fundamental potentials is multiplied by a certain weighting parameter to account for the contribution of the fundamental part to the overall potential. We may thus construct a phenomenological interaction potential model describing the physicochemical properties of the interaction of an oxygen atom with a material surface.

On account of the oxygen atoms in the LEO environment being characterized by high translational kinetic energies, and as very active oxidizing agents with capabilities of forming bonds of some atomic oxygen at a material surface, it is proposed here that the interaction potential between an oxygen atom and the material surface follows the concept of chemisorption. Thus, the UBI-QEP method can be employed to construct the fundamental potential between an incoming particle and a surface,[14] which is suitable, in principle, for the chemisorption process at any material surface. Accordingly, by denoting the fundamental potential as V_f, we have

$$V_f = Q_{\mathrm{oA}} \sum_{i=1}^{n} \left[x_i^2(r_i) - 2x_i(r_i) \right], \qquad x_i = \exp(-(r_i - r_e)/a) \tag{2}$$

where a is the range parameter, r_e the equilibrium distance, n the coordination number, and Q_{oA} the bond energy between a projectile and a single atom of the surface.

The range parameter a may be given by the relationship

$$r_n = r_0 + a\, \ell_n n \tag{3}$$

where r_n and r_0 are the equilibrium distances with respect to the coordination numbers n and 1, respectively. Q_{oA} can be obtained with the following set of relations:

$$Q_{n\mathrm{A}} = Q_{\mathrm{oA}} \left(2 - \frac{1}{n} \right), \qquad \Delta E_{\mathrm{dif}}^* = \gamma_n Q_{n\mathrm{A}}$$

$$\gamma_n = \frac{n-2}{4n-2}, \qquad n > 2$$

$$\Delta E_{\mathrm{app}}^* = \frac{\Delta E_{\mathrm{dif}}^* k_{\mathrm{int}} + \Delta E_{\mathrm{int}}^* D^*}{k_{\mathrm{int}} + D^*} \tag{4}$$

where $Q_{n\mathrm{A}}$ is the chemisorption heat, γ_n the corrugation ratio, $\Delta E_{\mathrm{app}}^*$ the apparent active barrier, $\Delta E_{\mathrm{dif}}^*$ the diffusion barrier, and $\Delta E_{\mathrm{int}}^*$ the intrinsic active barrier. Both D^* and k_{int} are defined based on the following reaction:

$$\mathrm{A} + \mathrm{B} \underset{D^*}{\overset{D}{\rightleftarrows}} \mathrm{A}^* + \mathrm{B}^* \xrightarrow{k_{\mathrm{int}}} \text{product}$$

where D and D^* are the diffusion constants for the adsorbates A + B and a corresponding precursor state $\mathrm{A}^* + \mathrm{B}^*$, respectively, and k_{int} is the intrinsic rate constant.[14] An apparent rate constant can then be defined as

$$k_{\mathrm{app}} = \frac{k_{\mathrm{int}} D}{D^* + k_{\mathrm{int}}}$$

The activation barrier for a process is related to the corresponding rate constant by assuming the Arrhenius forms:

$$k = A \exp\left(-\Delta E^* \big/ k_B T \right)$$

B. Deduction of Effective Potential Between Atomic Oxygen and Material Surface

As far as atomic oxygen effects are concerned, for nonreactive oxygen atoms, direct inelastic scattering occurs mainly on a material surface. In accordance with the model, constructed by Whitaker and Jang, for 19 polymeric materials (e.g., Kapton, polyethylene) exposed to a thermal atomic oxygen environment, the surface reaction is diffusion-controlled.[15] Therefore, $\Delta E_{\mathrm{dif}}^* \gg \Delta E_{\mathrm{int}}^*$, and it is reasonable to assume that $\Delta E_{\mathrm{app}}^* \cong \Delta E_{\mathrm{dif}}^*$ (Ref. 14). In addition, under the UBI-QEP approximation, the many-body effects for the simultaneous interaction of an incoming particle with multiple target particles on the surface can be confined within the range containing nearest target particles.

On the other hand, for high collision energies where the "structure" regime applies, the gas atoms experience a rougher potential dominated by the repulsive interaction with individual surface atoms, so that the predominant part of the potential is repulsive,[12,16] and the attractive part of the potential plays only a minor role. It is for this reason that we multiply the attractive part of the potential by a weighting factor ε_{gs} to reduce the influence of the attractive potential.

In addition, it is well known that the dynamical behavior of the atomic oxygen, together with its effects over the material surface in LEO environment, is rather complex. Various physical and/or chemical processes may arise from the collision of atomic oxygen with polymeric surfaces, such as 1) direct elastic scattering characterizing the specular scattering and diffraction; 2) direct inelastic scattering; 3) physisorption; 4) indirect scattering; and 5) reactive scattering of products through chemisorption. However, it is not realistic to attempt to express all the mechanisms involved in the processes mathematically and construct a general model for the interaction. Because the interaction itself is probabilistic in nature, and in accordance with the inherent high oxidizing capability of the atomic oxygen and the associated high translational energy, the chemisorption is irreversible. As for the interaction of a single atomic oxygen with a surface, and so far as the interaction governed by van der Waals forces or chemical bond forces is considered, it is not possible to identify a priori whether the equilibrium distance is characterized by the order of magnitude of the physisorption (about 10 au, i.e., atom unit) or the chemisorption (about 3 au), due to the probabilistic nature of the interaction process. Thus, the equilibrium distance for an incoming oxygen atom interacting with a material surface should be considered, in a statistical sense, as an intricate process covering from physisorption to chemisorption. In the present task, we define an equilibrium distance factor ε_e to account for the comprehensive effects stemmed from various processes.

By introducing these factors into potential (2) to form the interaction potential of an incoming oxygen atom with the particles of a material surface, we have

$$V_{\text{O–S}} = Q_{\text{oA}} \sum_{i=1}^{n} \left[x_i^2(r_i) - 2\varepsilon_{gs} x_i(r_i) \right], \qquad x_i = \exp \frac{-(r_i - \varepsilon_e r_e)}{a} \tag{5}$$

In principle, these two factors can be evaluated through fitting flight data or from ground tests.

III. Theoretical Formulation of Atomic Oxygen and Monomer Interaction

As an example, we present an analysis of the interaction between atomic oxygen and a Kapton surface. The multizone model[11] based on the theory of molecular dynamics is applied to simulate the interaction process. The interaction potential between the atomic oxygen and monomers of the Kapton surface can be deduced from Eq. (5), and the interaction potentials between monomers are readily given by Lifshitz's theory.[17] See Appendices A–D.

A. Governing Equations

Consider a general localized volume of a certain size and shape in the surface layer of a material, denoted by $V_>$. Define a subvolume $V_<$ of $V_>$ where dynamical characteristics are dominated by the effects of direct interaction between the atomic oxygen and the surface layer. Keeping in mind that the surface atoms described in Ref. 11 are now extended to include the macromolecules on the surface, such as the monomers of a polymeric surface, the dynamical interaction process for the entire system can be governed by the following set of equations[11]:

1. Dynamic Equations for Gas Particles

All motion of the gas particles follows the classical theory of molecular dynamics, that is,

$$M_g \frac{\mathrm{d}^2 \boldsymbol{X}}{\mathrm{d}t^2} = -\nabla_X V(\boldsymbol{X}, \boldsymbol{Y}_I, \boldsymbol{Y}_E, \boldsymbol{Y}_F) \tag{6}$$

where $\boldsymbol{X}$ is the coordinates of the gas particles and ∇_X denotes the gradient with respect to the coordinates of $\boldsymbol{X}$. It is seen that, in Eq. (6), we have made an assumption of neglecting collision between gas particles, because in LEO, the gas can be considered to be in the state of free molecular flow.

The dynamic equations for the monomers of a polymeric surface can be constructed in accordance with the multizone model on the surface layer of the solid in $V_>$.

2. Dynamic Equations for Particles in $V_<$ (Inner Zone)

The monomers in the inner zone $V_<$ are treated by standard molecular dynamics, and can be written as

$$M_s \frac{\mathrm{d}^2 \boldsymbol{Y}_I}{\mathrm{d}t^2} = -\nabla_{Y_I} V(\boldsymbol{X}, \boldsymbol{Y}_I, \boldsymbol{Y}_E, \boldsymbol{Y}_F) \tag{7}$$

3. Dynamic Equations for Particles in Edge Zone

The motions of the edge monomers follow a class of Langevin equations involving additional isotropic local frictional and Gaussian white-noise type random forcing terms, which can be written as

$$M_s \frac{\mathrm{d}^2 \boldsymbol{Y}_E}{\mathrm{d}t^2} = -\nabla_{Y_E} V(\boldsymbol{X}, \boldsymbol{Y}_I, \boldsymbol{Y}_E, \boldsymbol{Y}_F) - M_s \gamma \frac{\mathrm{d}\boldsymbol{Y}_E}{\mathrm{d}t} + \boldsymbol{f}_{Y_E}(t) \tag{8}$$

where

$$\gamma = \pi \omega_D / 6 = \pi k_B \theta_D / 6\hbar, \qquad \boldsymbol{f}_{Y_E}(t) = (2\gamma k_B T M_S / h)^{\frac{1}{2}} \xi_{Y_E} \tag{9}$$

Here, h is the time step in the integration, and the correlation of the frictional and random forces obeys the second fluctuation-dissipation theorem; that is,

$$\left\langle \boldsymbol{f}_{Y_E}(t) \boldsymbol{f}_{Y_E}(0)^T \right\rangle = 2\delta(t) \gamma M_S k_B T \overleftrightarrow{\mathbf{1}} \tag{10}$$

The proof of the second fluctuation-dissipation theorem clearly shows that the correlation between the dissipative and random forces can intimately be related to the requirement that the system relaxes to thermal equilibrium.

4. Fixed Monomers Zone ($V_> \cap \bar{V}_<$)

The monomers inside $V_>$ but external to $V_<$ are assumed to be unaffected by the interaction. They provide a structural template for the surface and smooth out the potential energy of the active monomers.

B. Interaction Potentials

Following Eq. (5), the interaction potential between an atomic oxygen and monomers in the surface layer of Kapton can be written as

$$V_{\text{O–PM}} = Q_{\text{oA}} \sum_{i=1}^{n} \left[x_i^2(r_i) - 2\varepsilon_{gs} x_i(r_i) \right]$$

$$x_i = \exp \frac{-(r_i - \varepsilon_e r_e)}{a} \tag{11}$$

with $Q_{\text{oA}} = 1.52$ eV, $a = 0.2051$ Å, $r_e = r_0 = 1.12058$ Å, where the derivations are given in Appendix A.

For molecular dynamic simulation of macromolecules, it is impractical to directly calculate the interaction potential between monomers with large molar mass (e.g., the system consisting of hundreds of atoms) via quantum mechanics.[6] The interaction potential within macromolecules can be constructed traditionally by uncoupling the interaction into bond stretching, bond angular bending, electrostatic interactions, torsional rotations, and van der Waals potentials, without considering the coupling interactions and many-body effects. Although a broadly applicable class II force field has been developed to account for the coupling interactions, it is necessary to perform the quantum mechanical computations to derive the force field parameters.[18] Lifshitz theory, on the other hand, has an advantage over this approach in dealing with the overall effects for the process of interaction between monomers, because the nonadditivity

problem on the free energy of a body system is completely overcome by that theory.[17] In the present work, we follow the Lifshitz theory to construct the effective attractive potential among the Kapton monomers. From Eq. (C4), we have

$$U'_{\mathrm{Lif}} = -44350.861/r^6\ (\mathrm{eV}\cdot\mathrm{\AA}^6) \tag{12}$$

According to the hypothesis for the effective potential based on a 12–6 Lennard–Jones power law, and the interaction energy $\varepsilon_{\mathrm{PM}} = 0.5182$ eV for Kapton monomers,[19] Eq. (12) gives the equilibrium distance $r_{e-\mathrm{PM}} = 5.269$ Å. Thus, the effective potential can be expressed as

$$U_{E-\mathrm{PM}} = 4\varepsilon_{\mathrm{PM}}\left[(r_{e-\mathrm{PM}}/r)^{12} - (r_{e-\mathrm{PM}}/r)^6\right] \tag{13}$$

where r is the distance between lattice points based on the simple model of polymers.

C. Debye Temperature

To estimate the dissipative effect of the particles inside the edge zone,[11] the Debye model based on the theory of heat capacity is adopted to evaluate the Debye temperature for the material under consideration and the associated frictional coefficients, without considering the atomic structure of the solid medium. The Debye temperatures of materials may be estimated by various approaches, such as specific heat, melting point, compressibility, velocity of sound, and the infrared spectrum.[20] In the present paper, the Debye temperature of Kapton is evaluated using the average sound velocity, which gives $\theta_D = 165$ K (cf. Appendix D).

D. Reactive Criterion

Following the classical trajectory approach for the reaction dynamics, the reactive criterion, also termed as the impact parameter, can be defined in different ways, such as by quantizing the initial orbital angular momentum at a given relative velocity.[21,22] In our case, for the interaction of an atomic oxygen with a polymeric surface, owing to the intimate relationship between the reactive criterion and chemisorption, it is defined in accordance with the properties related to chemisorption, including the appearance of shared electrons belonging both to the adsorbate and to the substrate, as well as the bond formation of the adsorbate at the surface.

With regard to the potential-energy function of the adsorbate–adsorbent system, its minima reflect the intermediate steps of a certain chemisorption process. The absolute minimum defines the equilibrium state for the geometrical structure, and thus the binding energy as well. The curvature around the minimum gives the vibrational frequency of the system.[23] Hence, from the relation between the geometrical structure (e.g., the bond length) of the system and the absolute minimum of the potential energy surface, one can correlate the reactive criterion with the bond length of a bond formation. It is not possible in the present stage to describe either theoretically or experimentally the complete process for the chemisorption, nor to calculate the bond length accurately. On the basis of the experimental data for the atomic-oxygen chemisorption on the surfaces of Ni, Al, and so forth,[24,25] we propose here that, when the distance of an incoming particle perpendicular to the surface is equal to half of the bond length, chemisorption takes place. The distance from the projectile particle to the nearest-neighbor particle at the surface is assumed to be the bond length, and the potential energy takes its minimum at the onset of chemisorption. As a result, in the present work we define the reactive criterion to be half of the bond length whenever the adsorbate forms a bond at the surface.

According to this criterion, the onset of the chemisorption of an oxygen atom onto a Kapton surface is given as $r_c = 0.7025$ Å for all computations involved.

The reactive probability can be defined as the ratio between the number of the reactive events N_R and the total number of trajectories N_T (Ref. 11), namely,

$$P_R = \frac{N_R(r_c;\, E_i;\, \theta_k)}{N_T(r_c;\, E_i;\, \theta_k)} \tag{14}$$

where θ_k is the specific incident angle of the incoming particle. For nonreactive trajectories, the energy accommodation coefficient (EAC) may be defined as[26,27]

$$\alpha = \frac{\bar{E}_i - \bar{E}_f}{\bar{E}_i - 2k_B T_S} \tag{15}$$

When the energy accommodation coefficients are averaged over all of the nonreactive trajectories for various incident angles, the average EAC is given by

$$\langle\alpha\rangle = \frac{1}{N_T - N_R}\sum_{i=1}^{N_T - N_R}\alpha_i \tag{16}$$

where α_i denotes the energy accommodation coefficient of the ith nonreactive trajectory.

IV. Method of Solution and Numerical Results

The governing system of Eqs. (6–8) with both the interaction potentials and the Debye temperatures for materials deduced above are solved by the standard Verlet algorithm to give the trajectories for the sample particles.[28] Thus, we may trace the trajectories of the projectile particles in accordance with the specified reaction criterion. When the particle makes a bond at the surface, the trajectory is termed a reactive trajectory. When only a physical process takes place, the trajectory is called a nonreactive trajectory. Finally, the reactive probability and the energy accommodation factor can be computed by Eqs. (15) and (16).

A. Given Conditions for Numerical Test Case

The high-order lattice structure for Kapton belongs to the orthorhombic cells as shown in Fig. 1, whose lattice parameters are $a = 6.3$ Å, $b = 4.0$ Å, and $c = 32$ Å (Ref. 29). The Kapton monomers occupy the cubic lattice points based on the simple lattice model of polymers.[30] Hence, the distance between the adjacent lattice points can be calculated from its lattice structure and lattice parameters to be 5.8636 Å.

To provide the initial conditions for the distribution of particle velocities in the polymer surface, a few layers of Kapton monomers under thermal equilibrium at a certain temperature must be obtained. The system considered in the present computations consists of an oxygen atom and six layers of Kapton monomers. The initial translation energy of an oxygen atom is set to be 5 eV. Then the initial velocity vector of an oxygen atom can be determined via initial translation kinetic energy, the polar angle from the surface normal

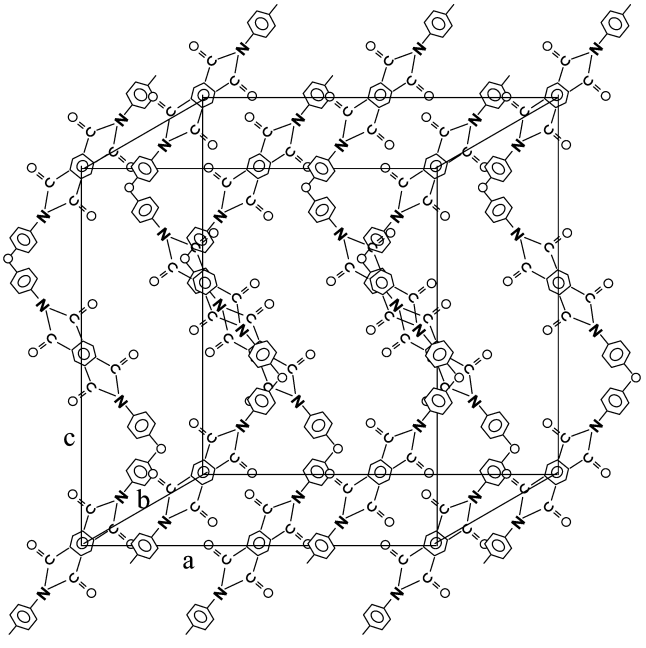

Fig. 1 Lattice structure of Kapton.

axis, θ, which is equal to the incident angle for each case, and the azimuthal angle from the x axis where $\phi = 0$. The specified value of the initial height above the surface is 14 Å, and the initial position is randomly sampled over the substrate lattice. The positions of Kapton monomers located at the lattice points are initialized using a method of molecular dynamics; their initial velocities are sampled from a Maxwell–Boltzmann distribution for $T_s = 310$ K (Ref. 31). The Miller index for the lattice surface of Kapton is (100).

When the incident angles of the incoming atomic oxygen vary from 0 to 70 deg, the volume $V_>$ used in the calculations contains 394 inner, 897 edge, and 2579 fixed monomers. When the incident angles are larger than 70 deg, there are 10 inner, 449 edge, and 3411 fixed monomers used in the calculations due to the fact that the surface response of the incoming particle becomes weakened here. The interaction potential of an oxygen atom with a lattice surface of the Kapton and the effective potential between Kapton monomers will be computed using Eqs. (11) and (13), respectively, whereas the threshold of the interaction potential is readily given as $r_{\text{crit}} = 16$ Å, and the Debye temperature is $\theta_D = 165$ K.

The time step for integrating the equations of motion is set to be 0.2 fs. At each integration step, the random forces $\boldsymbol{f}_{Y_E}(t)$ appearing in Eq. (8) are randomly selected from a Gaussian distribution given by the second equation (9). We use 1000 sample oxygen atoms at each incident angle to obtain the required statistical properties. The reactive criterion $r_c = 0.7025$ Å.

B. Numerical Results

The reactive probabilities for various incident angles and the average reactive probability for given ε_e and ε_{gs} are summarized in Table 1, together with the data collected for an atomic-oxygen etching on a Kapton surface during the STS-46 mission.[8] Similarly, EAC for various incident angles and the average EAC for given ε_e and ε_{gs} are summarized in Table 2.

The bond energies for C–N, C–C, C–H, and C–O bonds for Kapton are about 3.16, 3.58, 4.24, and 3.70 eV, respectively.[32] As for the specimens erosion efficiency $P_{R-\text{LEO}}$ measured in the ram attitude within ±5 deg; however, Catherine (cited in Ref. 4) shows that the required energy to create erosion due to a collision is approximately three times the bond energy. As a result, the spalling effects on the Kapton surface cannot occur because O-atoms with translational energy 5 eV are unable to provide sufficient energy to break the bonds stated above. The chemical reactions of atomic oxygen on the Kapton surface play a key role in giving rise to the mass loss of Kapton. Therefore, the erosion efficiency of atomic oxygen on the Kapton surface in LEO, $R_e = 3.1 \times 10^{-24}$ cm^3/atom, is taken as the reactive probability of atomic oxygen on the Kapton surface, that is, $P_{R-\text{LEO}}$.

According to Eq. (A1), the chemical reaction caused by the atomic oxygen is given as

$$C_{22}H_{10}O_5N_2 + 35O \rightarrow 11CO_2 + 11CO + 5H_2O + 2NO$$

that is, one Kapton monomer reacts with 35 oxygen atoms. For $M_S = 382.3$ au, $\rho = 1.41$ g/cm^3, we have $P_{R-\text{LEO}} = 35R_e/[M_S/(\rho N_A)] \approx 0.2409$.

C. Analysis and Discussion

Because the microroughness of the material surface and the thermal motion of atomic oxygen make the ram reactive probability in the ram attitude within ±5 deg favorable toward its azimuthal average value, the average reactive probability computed by the method proposed in the present work is compatible with those obtained from the flight data. Accordingly, the value of the average reactive probability computed for the test case is readily given as 0.2003 (as listed in the first set of factors in Table 1), which is less than the flight data of 0.2409, as mentioned above. The simulated result is reliable because the laboratory result showed a synergistic effect of atomic oxygen and electron radiation for Kapton.[33]

The average EAC computed by the present test case is 0.1368 (as listed in the first set of factors in Table 2), which lies between 0.1165, obtained by the hard-sphere model,[27] and 0.68, given by

Table 1 Reactive probabilities for different factors and STS-46 flight experiment[a]

			Adjustable factors				
ε_e	2.9	3.0	3.0	3.0	3.0	2.9	3.1
ε_{gs}	0.2	0.2	0.25	0.35	0.68	0.0	0.2
				P_R			
θ, deg							
0	0.335	0.256	0.267	0.261	0.28	0.338	0.218
10	0.327	0.262	0.253	0.258	0.29	0.322	0.229
20	0.288	0.238	0.229	0.242	0.243	0.303	0.191
30	0.241	0.23	0.228	0.221	0.219	0.251	0.167
40	0.233	0.154	0.173	0.205	0.198	0.185	0.13
50	0.161	0.127	0.115	0.148	0.187	0.157	0.074
60	0.105	0.065	0.084	0.093	0.135	0.077	0.05
70	0.084	0.042	0.05	0.056	0.126	0.048	0.017
80	0.029	0.013	0.019	0.035	0.09	0.0	0.002
$\langle P_R \rangle$	0.2003	0.1541	0.1576	0.1688	0.1964	0.1868	0.1198
$P_{R-\text{LEO}}$				0.2409			

[a] P_R are the computed values, $\langle P_R \rangle$ the computed average values. $P_{R-\text{LEO}}$ is flight data.

Table 2 EAC for different factors

			Adjustable factors				
ε_e	2.9	3.0	3.0	3.0	3.0	2.9	3.1
ε_{gs}	0.2	0.2	0.25	0.35	0.68	0.0	0.2
				α			
θ, deg							
0	0.186	0.1834	0.1828	0.1848	0.1884	0.187	0.176
10	0.184	0.176	0.1804	0.18	0.188	0.1798	0.1754
20	0.1774	0.1756	0.175	0.1764	0.1856	0.1766	0.1732
30	0.1684	0.171	0.1684	0.1702	0.179	0.167	0.171
40	0.1624	0.1572	0.157	0.1596	0.1668	0.1576	0.1548
50	0.147	0.1426	0.1446	0.144	0.1526	0.1434	0.1448
60	0.123	0.1234	0.1202	0.1262	0.1338	0.12	0.1214
70	0.0889	0.0904	0.0926	0.098	0.1144	0.0824	0.0878
80	0.0442	0.0444	0.0506	0.0576	0.094	0.0288	0.0218
$\langle \alpha \rangle$	0.1368	0.1360	0.1369	0.1402	0.1533	0.1313	0.1322

the ground-simulated experiments on the atomic oxygen with an incident angle of 45 deg and energy of 1.5 eV (Ref. 33). Hence, the EAC value computed in the present test case is reasonable. Larger measurable error for EAC data is found to be $0.6 \pm 50\%$ from ground tests using 8 km/s atomic oxygen impacting on nickel, gold, and curved glass performed by Krech et al.[34]

In fact, the impact of an incoming particle onto the material surface is not directed toward the entire monomer but part of it. The experiment confirms the fact that the application of the hard-sphere model is not suitable for estimating the EAC of an incoming particle impacting on a polymer surface. The effective mass of the surface collision partner (termed the surface effective mass) is introduced to modify the formula for EAC calculation in the hard-sphere model to fit the experimental data.[35] As mentioned, in the present work, we have simplified the structure of Kapton as a simple lattice without taking the concept of the surface effective mass into consideration. In addition, we have treated the surface of Kapton as an ideal surface, that is, a surface layer with an ordered structure, instead of a real material surface. These simplifications cause the numerical value computed by the present work for average EAC to be less than the experimental data.

The effects of the incident angle upon the reactive probability calculated in the present model are shown in Figs. 2a–8a. It is seen that the increment of the incident angle weakens the interaction between the incident oxygen atom and a material surface, reduces the energy transfer efficiency of the incident oxygen atom onto the surface, and makes the bond formation between atomic oxygen and surface monomers (i.e., production of shared electrons belonging to both the incident oxygen atom and the Kapton surface) more difficult.

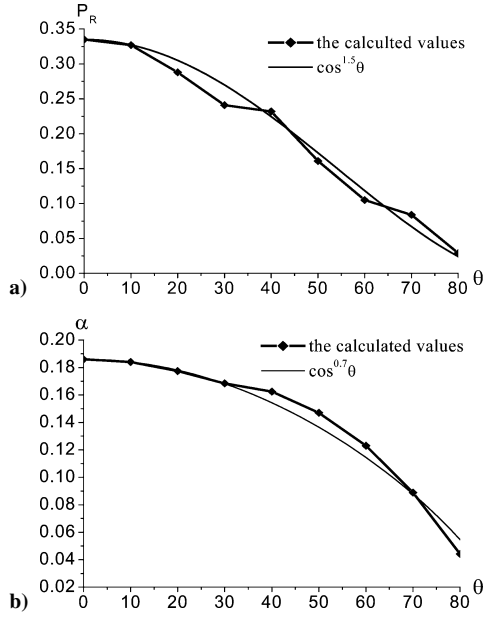

Fig. 2 Incident angle-dependence of a) reaction probability and b) energy accommodation coefficient for $\varepsilon_{gs} = 0.20$, $\varepsilon_e = 2.9$.

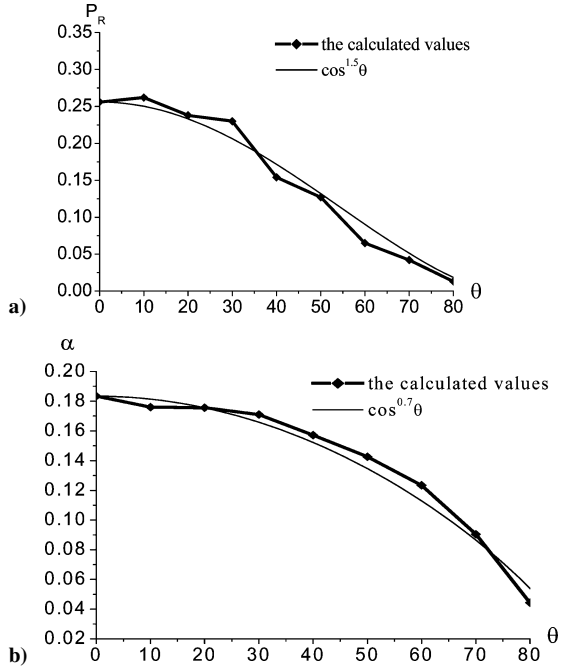

Fig. 3 Incident angle-dependence of a) reaction probability and b) energy accommodation coefficient for $\varepsilon_{gs} = 0.20$, $\varepsilon_e = 3.0$.

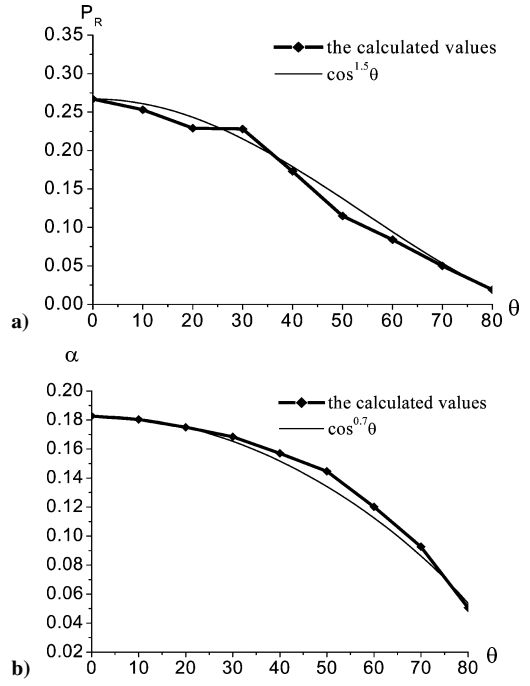

Fig. 4 Incident angle-dependence of a) reaction probability and b) energy accommodation coefficient for $\varepsilon_{gs} = 0.25$, $\varepsilon_e = 3.0$.

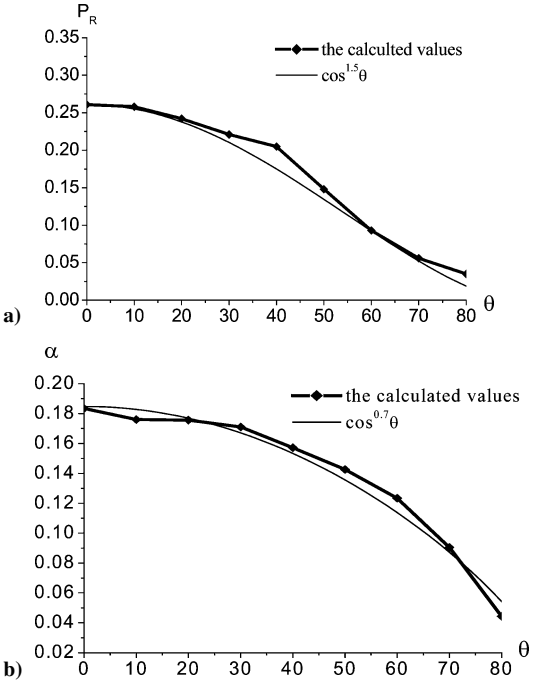

Fig. 5 Incident angle-dependence of a) reaction probability and b) energy accommodation coefficient for $\varepsilon_{gs} = 0.35$, $\varepsilon_e = 3.0$.

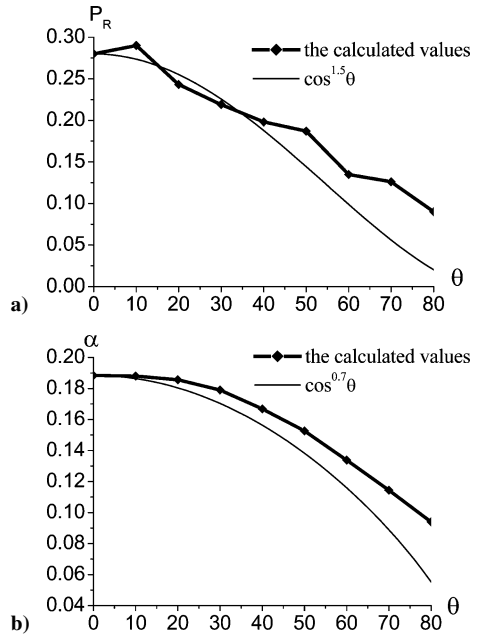

Fig. 6 Incident angle-dependence of a) reaction probability and b) energy accommodation coefficient for $\varepsilon_{gs} = 0.68$, $\varepsilon_e = 3.0$.

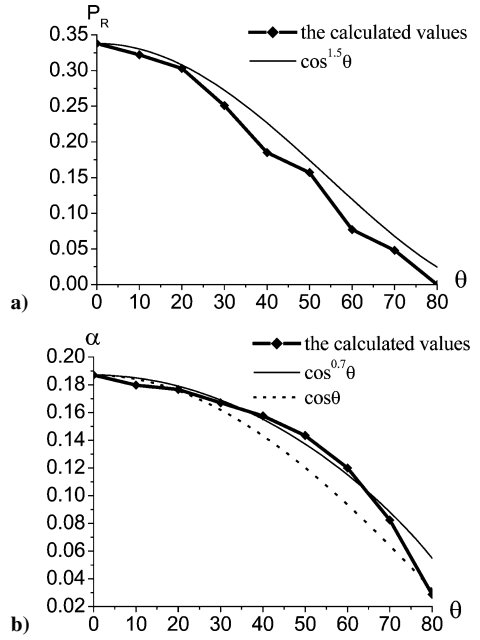

Fig. 7 Incident angle-dependence of a) reaction probability and b) energy accommodation coefficient for $\varepsilon_{gs} = 0.0$, $\varepsilon_e = 2.9$.

As shown in the figures, the fitted curve for the dependencies of the reactive probability on the incident angle agrees well with $\cos^{1.5}\theta$, which is given by the STS-8 flight experiment,[36] rather than $\cos\theta$ for the ground-based experimental results of Yokota et al.[37] The curves in Figs. 2b–8b fitted for the energy accommodation coefficient reveal, on the other hand, that the incident angle-dependency of EAC does not vary with $\cos\theta$ as characterized by the hard-sphere model,[27] but depends on $\cos^{0.7}\theta$ for the present work. The discrepancy between the two approaches stems from the different potential models. The potential proposed in the present work is constructed with a potential well having an equilibrium distance of the order of magnitude of chemisorption, about 3 au, instead of physisorption, with an equilibrium distance of about 10 au. Under such circumstances, the potential for chemisorption is dominated by its repulsive part. The different target materials used for the two models may also induce certain discrepancies.

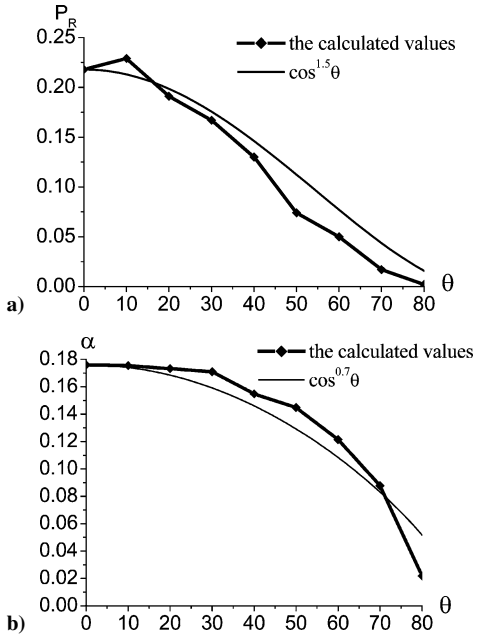

Fig. 8 Incident angle-dependence of a) reaction probability and b) energy accommodation coefficient for $\varepsilon_{gs} = 0.2$, $\varepsilon_e = 3.1$.

The data listed in Tables 1 and 2 demonstrate that the average reactive probability and average EAC drop as ε_{gs} decreases, due to the increment of repulsive force between an oxygen atom and surface particles. On the other hand, the reduction of ε_e may suppress the repulsive range between an oxygen atom and the Kapton surface and extend the attractive region. As a result, the reduction of ε_e promotes the chance for the atomic oxygen to form a bond at the surface, that is, leads to an increment of the reactive probability of the interaction, and also increases the average EAC in a small amount.

In addition, the reactive probability computed using the first set of factors in Table 1 is closer to its measured value than the ones using the remaining sets of factors. The first set of factors was inversely deduced from experimental data fitting. For comparison, we perform further numerical calculations with six additional sets of factors chosen at random. These results are also given in Table 1. The differences among the numerical results indicate that the two factors ε_e and ε_{gs} do possess their respective physical significances as discussed in Sec. II.B, and can only be obtained via empirical means at present. As shown in Fig. 6a, the value ε_{gs} should not exceed 0.68; otherwise the curves fitted for the incident angle vs the reactive probability will not follow the $\cos^{1.5}\theta$ law.

V. Conclusions

In the present paper, an interaction potential model for an incoming particle impacting a polymeric material surface is developed and applied to estimate the reactive probability and energy accommodation coefficient for Kapton. The reactive probability computed by the present model is found to be 16.8% less than the flight experimental data from STS-46, whereas the value of the EAC computed with the present model lies in the range between the value using the hard-sphere model and the experimental data.

Numerical experiments confirm the law of dependency of the reactive probability upon the incident angle deduced from the flight experiments. Different cosine power laws for the dependency of EAC upon the incident angle characterized by different powers between incoming particles impacting the polymer surface and the metal surface have also been found in the present study.

Appendix A: Interaction Potential Between an Atomic Oxygen and Monomers in the Surface Layer of Kapton

By applying the apparent active energy of atomic oxygen on a Kapton surface[38] and relation (4), we obtain $E_a = \Delta E^*_{\text{app}} = \Delta E^*_{\text{dif}} = 0.38$ eV.

Although the dynamical behavior of atomic oxygen interacting with the Kapton surface is so complex that the coordination number of the atomic oxygen stays undetermined, it may be estimated based on the highly ordered structure of Kapton. The preferred binding site of an oxygen atom with the nearest-neighbor monomers is theoretically available; the number of monomers of the kind depends on the symmetry of the material structure. When we apply lattice structure with orthorhombic cells to model Kapton,[29] $n=4$ if its Miller indices are (100); and Eq. (4) gives $Q_{\mathrm{oA}}=1.52$ eV. To estimate the range parameter a, it is necessary to make the following assumptions.

First, because the exact orders of the reaction process on oxygen atoms with Kapton monomers as well as the reactant species are still unclear,[39] the theoretical reactive model between atomic oxygen and Kapton monomer is deduced from the Skurat model,[40]

$$\mathrm{C_{22}H_{10}O_5N_2 + 24O \rightarrow 22CO + 5H_2O + 2NO}$$

$$\mathrm{C_{22}H_{10}O_5N_2 + 46O \rightarrow 22CO_2 + 5H_2O + 2NO}$$

with the data of mass spectrometry for the reactants,[8] and is given as

$$\mathrm{C_{22}H_{10}O_5N_2 + 35O \rightarrow 11CO_2 + 11CO + 5H_2O + 2NO} \quad \text{(A1)}$$

Second, following the experimental data,[39] we may assume that the reaction between the oxygen atom and Kapton monomer forms CO_2.

Third, according to the frontier orbital theory,[41,42] we assume that the initial step for chemisorption is the formation of the single bond between an atomic oxygen and a certain atom of a Kapton monomer.

According to the stated considerations, incorporating with weighted technique, the "average" bond length can be estimated via formula (B3) as

$$D(\mathrm{O{-}E}) = r_E + r_{\mathrm{O}} - 0.019|\chi_{\mathrm{O}} - \chi_{\mathrm{PM}}| \quad \text{(A2)}$$

where $E=$ C, H, N; N_{O} and N_P ($P=\mathrm{CO_2}$, CO, NO, $\mathrm{H_2O}$) are the stoichiometric coefficients of the atomic oxygen and the productions in the gross equations of oxidation (A1), respectively; and r_{O} and $r_E(E=\mathrm{C, H, N})$ denote the covalent radii of both the atomic oxygen and the atom on a Kapton surface, respectively (cf. Table A1).[43] The electronegativity of the atomic oxygen is readily given as $\chi_{\mathrm{O}}=7.54$ eV,[44] and the electronegativity for the Kapton monomer, computed by its ionization potential $I=9.1$ eV and electron affinity $\mathrm{EA}=2$ eV,[45] as $\chi_{\mathrm{PM}}=(I+\mathrm{EA})/2=5.55$ eV. As a result, we have

$$D(\mathrm{O{-}C}) = 1.4742\ \text{Å}, \qquad D(\mathrm{O{-}N}) = 1.4422\ \text{Å}$$

$$D(\mathrm{O{-}H}) = 1.0022\ \text{Å}$$

$$\langle D(a-s)\rangle = \frac{2N_{\mathrm{CO_2}}-5}{N_{\mathrm{O}}}\times D(\mathrm{O-C}) + \frac{N_{\mathrm{CO}}}{N_{\mathrm{O}}}\times D(\mathrm{O{-}C}) + \frac{N_{\mathrm{NO}}}{N_{\mathrm{O}}}\times D(\mathrm{O-N}) + \frac{N_{\mathrm{H_2O}}}{N_{\mathrm{O}}}\times D(\mathrm{O-H})$$

$$\langle D(a-s)\rangle = 1.40491\ \text{Å}$$

Similarly, according to the bond lengths between atoms of every product listed in Table A2,[46] $\langle r_0\rangle$, instead of r_0 in Eq. (3), is obtained by the following relation based on the weighted method:

$$\langle r_0\rangle = \frac{2N_{\mathrm{CO_2}}-5}{N_{\mathrm{O}}}\times r_{\mathrm{C_2O}} + \frac{N_{\mathrm{CO}}}{N_{\mathrm{O}}}\times r_{\mathrm{CO}} + \frac{N_{\mathrm{NO}}}{N_{\mathrm{O}}}\times r_{\mathrm{NO}} + \frac{N_{\mathrm{H_2O}}}{N_{\mathrm{O}}}\times r_{\mathrm{H_2O}} = 1.12058\ \text{Å}$$

Table A1 Covalent radii for atoms

Bond type	H	C	N	O
Single	0.3	0.772	0.74	0.74
Double	—	0.667	0.62	0.62
Triple	—	0.603	0.55	0.55

Table A2 Bond lengths for molecules

Molecule	Bond length
O=C=O	1.1600
C≡O	1.1283
N=O	1.1506
H_2O	0.9575

Here, $\langle D(a-s)\rangle = r_n$; thus we have $a=[\langle D(a-s)\rangle - \langle r_0\rangle]/\ell_n\, n = 0.2051$ Å.

Finally, the potential between an oxygen atom and Kapton monomers can be obtained as

$$V_{\mathrm{O-PM}} = Q_{\mathrm{oA}}\sum_{i=1}^{n}\left[x_i^2(r_i) - 2\varepsilon_{gs}x_i(r_i)\right]$$

$$x_i = \exp(-(r_i - \varepsilon_e r_e)/a) \quad \text{(A3)}$$

where $Q_{\mathrm{oA}}=1.52$ eV, $a=0.2051$ Å, $r_e=r_0=1.12058$ Å.

Appendix B: Bond Length of the Chemisorption of an Oxygen Atom on the Polymer Surface

An available empirical formula for evaluating bond length is extended to predict the bond length formed by the interaction between space particles and material surfaces. By employing the concept of electronegativity proposed by Pauling in 1932 (Ref. 47), Schomker and Stevenson[48] propose an empirical formula for estimating the bond length as

$$D(\mathrm{A-B}) = r_{\mathrm{A}} + r_{\mathrm{B}} - c|\chi_{\mathrm{A}} - \chi_{\mathrm{B}}| \quad \text{(B1)}$$

where $r_{\mathrm{A}}, r_{\mathrm{B}}$ are the covalent radii, and $\chi_{\mathrm{A}}, \chi_{\mathrm{B}}$ the electronegativities of atoms A and B, respectively; c is the Schomker–Stevenson coefficient, whose value is given as 0.09 Å. The later works by Pauling, Polansky, and Derflinger and others are then focused on the modification of the coefficient.[43,49]

Equation (B1) is extended to the chemisorption on semiconductors by Mönch,[50] and can be rewritten as

$$D(a-s) = r_a + r_s - \mathrm{c}_{as}|\chi_a - \chi_s| \quad \text{(B2)}$$

where r_a, r_s are the covalent radii and χ_a, χ_s the electronegativities of the adsorbate and the surface atom, respectively, and the Schomker–Stevenson coefficient c_{as} varies from 0.02 through 0.06 Å/eV.

Bergmann et al. perform a statistical investigation for the 122 bonds of 122 compounds and determine the Schomker–Stevenson coefficient $c=(1.9\pm0.2)\times10^{-2}$ Å/eV via a least-squares regression.[51] In the present work, we adopt formula (B2) with Schomker–Stevenson coefficient c_{as} given by Bergmann et al. for evaluating the bond length of the chemisorption of an oxygen atom on the polymer surface, namely,

$$D(\mathrm{O-S}) = r_{\mathrm{O}} + r_{\mathrm{S}} - 0.019|\chi_{\mathrm{O}} - \chi_{\mathrm{S}}| \quad \text{(B3)}$$

Appendix C: Effective Attractive Potential for Kapton

The interaction potential between monomers in the polymeric material surface layers is deduced based on the following effective attractive potential[17]:

$$U_{\mathrm{Lif}} = -\left[\frac{2\left(\omega_1^0+\omega_2^0\right)(\varepsilon_{\infty1}+2)(\varepsilon_{\infty2}+2)}{9\pi\left(\omega_1^0-\omega_2^0\right)}\,\ell_n\left(\frac{\omega_1^0}{\omega_2^0}\right)\right] \times \frac{3\hbar}{2r^6}\frac{\omega_1^0\omega_2^0}{\omega_1^0+\omega_2^0}\alpha_1\alpha_2 \quad \text{(C1)}$$

For the case of identical molecules, we have

$$U'_{\mathrm{Lif}} = -(4/\pi)[(\varepsilon_\infty+2)/3]^2(3\hbar/4r^6)\omega^0\alpha^2 \quad \text{(C2)}$$

where ω_i^0 ($i=1, 2$) are the characteristic absorption frequencies, and $\varepsilon_{\infty i}$ ($i=1, 2$) the optical dielectric constants of media 1 and

2, respectively; α_i ($i = 1, 2$) the polarizabilities of molecules (or atoms) 1 and 2, respectively; r represents the distance between the molecules (or atoms), $\hbar$ denotes the Dirac constant, and $\alpha = \alpha(0)$.

As for Kapton monomers, $\alpha(0)$ is replaced by $\bar{\alpha}$ through the Lorenz–Lorentz equation,

$$R = [(n^2 - 1)/(n^2 + 2)](M_0/\rho) = \tfrac{4}{3}\pi N_A \bar{\alpha} \tag{C3}$$

where R is the molecular refraction, n the refraction index, ρ the density, and M_0 the molar mass. The molecular refraction R can be obtained experimentally to be 106×10^{-6} m^3 (cf. Ref. 52), and thus $\bar{\alpha} = 42.023$ Å^3. In addition, $\varepsilon_\infty = 3.1$ (cf. Ref. 53), and the ionic energy for the Kapton monomer is given as $I = 9.1$ eV (Ref. 45). Hence, from Eq. (C2) we have

$$U'_{\text{Lif}} = -44350.861/r^6 \ (\text{eV} \cdot \text{Å}^6) \tag{C4}$$

Appendix D: Debye Temperature of Kapton

The expression of θ_D related to the average sound velocity v_{av} is readily given as

$$\theta_D = (h/k_B)[(3q/4\pi)(N_A\rho/M)]^{\frac{1}{3}} v_{\text{av}} \tag{D1}$$

where h is Planck's constant, N_A the Avogadro number, ρ the density, M the molar mass of the solid, and q the number of atoms in the molecule.[54] The average sound velocity v_{av} is given by integrating the three sound velocity components along all directions as

$$v_{\text{av}} = \left(\frac{1}{3}\sum_{i=1}^{3}\int_0^{4\pi}\frac{1}{v_i^3}\frac{\mathrm{d}\Omega}{4\pi}\right)^{-\frac{1}{3}} \tag{D2}$$

where v_i are the velocity components of the elastic waves propagation in the media at 0 K, and $\mathrm{d}\Omega$ denotes an element of the solid angle. For isotropic solids, relation (D2) reduces to

$$v_{\text{av}} = \left(\tfrac{1}{3}\left[2/v_t^3 + 1/v_l^3\right]\right)^{-\frac{1}{3}} \tag{D3}$$

where v_t and v_l are the longitudinal and transversal sound velocities, respectively.[55]

For polycrystalline solids, due to the fact that the values of v_t and v_l obtained by the experiments and the values of $\bar{v}_t$ and $\bar{v}_l$ obtained by averaging the elastic constants for single crystals are almost the same, we thus assume that the averaged velocities defined in Eq. (D3) can be replaced by $\bar{v}_{\text{av}}$ (Ref. 54); we have

$$\bar{v}_{\text{av}} = \left(\tfrac{1}{3}\left[2/\bar{v}_t^3 + 1/\bar{v}_l^3\right]\right)^{-\frac{1}{3}} \tag{D4}$$

It should be pointed out that the value obtained from Eq. (D4) would be slightly different from the value v_{av} calculated by the rigorous method, that is, the relation (D2).

As for Kapton, the values of $\bar{v}_{\text{av}}$ and θ_D can be evaluated through its bulk and shear moduli. There are various theoretical models available for estimating the bulk and shear moduli. By comparing with the Reuss model, the elastic modulus of Kapton predicted by the Voigt model is found to be closer to the experimental value.[56] Thus, we adopt the Voigt model in the present paper. By virtue of the Voigt model,[57] we have

$$K_V = [(c_{11} + c_{22} + c_{33}) + 2(c_{12} + c_{23} + c_{13})]/9 \tag{D5}$$

$$G_V = [(c_{11} + c_{22} + c_{33}) - (c_{12} + c_{23} + c_{13}) + 3(c_{44} + c_{55} + c_{66})]/15 \tag{D6}$$

where c_{ij} denote the stiffness coefficients, and K_V and G_V are the Voigt approximation of the bulk and shear moduli, respectively. The expressions for $\bar{v}_t$ and $\bar{v}_l$ in terms of K_V and G_V are given as

$$\bar{v}_t = \sqrt{G_V/\rho} \tag{D7}$$

$$\bar{v}_l = \sqrt{(K_V + 4/3G_V)/\rho} \tag{D8}$$

Table D1 Kapton's θ_D and its correlative data

Parameters	Value
K_V, kbars	77.108
G_V, kbars	17.2132
$\bar{v}_t$, m/s	1140.89
$\bar{v}_l$, m/s	2663.9
$\bar{v}_{\text{av}}$, m/s	1250.09
θ_D, K	165

According to the compliance matrix for Kapton,[56] we have

$$s_{ij} = \begin{bmatrix} 15.85 & -7.88 & -3.33 & 0 & 0 & 0 \\ -7.88 & 17.51 & -3.33 & 0 & 0 & 0 \\ -3.33 & -3.33 & 9.17 & 0 & 0 & 0 \\ 0 & 0 & 0 & 50.76 & 0 & 0 \\ 0 & 0 & 0 & 0 & 204.08 & 0 \\ 0 & 0 & 0 & 0 & 0 & 370.37 \end{bmatrix} \times 10^{-2} \ (m^2/GN)$$

and the relationship between the compliance and stiffness matrices is given as

$$S_{ij} = (C_{ij})^{-1} \tag{D9}$$

where $(C_{ij})^{-1}$ is the inverse of the stiffness matrices. Applying Eqs. (D5–D9), (D4), and (D1), we may obtain the results shown in Table D1.

Experimental information is not available on the Debye temperature of Kapton at present. The value of θ_D for Kapton given in Table D1 is a computed value and remains to be verified experimentally.

Acknowledgments

The present work was supported by China National Science Foundation. We are deeply indebted to David L. Edwards, an Associate Editor for the *Journal of Spacecraft and Rockets*, for improving the grammar of the manuscript. We express our thankfulness to the reviewers for their comments.

References

[1]Levine, A. S. (ed.), "LDEF–69 Months in Space," 1st Post-Retrieval Symposium, NASA CP-3134, June 1991, pp. 617–642.

[2]Leger, L. J., "Oxygen Atomic Reaction with Shuttle Materials at Orbital Altitudes," NASA TM-58246, May 1982.

[3]Singh, B., Amore, L. J., Saylor, W., and Racette, G., "Laboratory Simulation of LEO Atomic Oxygen Interaction with Spacecraft Surfaces," AIAA Paper 85-0477, Jan. 1985.

[4]Cazaubon, B., Pailous, A., Sffre, J., and Thomas, R., "Mass Spectrometric Analysis of Reaction Products of Fast Oxygen Atoms–Material Interactions," *Journal of Spacecraft and Rockets*, Vol. 35, No. 6, 1998, pp. 797–804.

[5]Zhao, X.-H., Shen, Z. G., Xing, Y. S., and Ma, S.-L., "A Study of the Reaction Characteristics and Mechanism of Kapton® in Plasma-Type Ground-Based Atomic Oxygen Effects Simulation Facility," *Journal of Physics D*, Vol. 34, No. 15, 2001, pp. 2308–2314.

[6]Troya, D., and Schatz, G. C., "Theoretical Studies of Hyperthermal O(^{3}P) Collisions with Hydrocarbon Self-Assembled Monolayers," *Journal of Chemical Physics*, Vol. 120, No. 16, 2004, pp. 7696–7707.

[7]Snyder, A., and Banks, B. A., "Fast Three-Dimensional Method of Modeling Atomic Oxygen Undercutting of Protected Polymers," NASA TM-211578, May 2002.

[8]Koontz, S. L., Leger, L. J., Visentine, J. T., Hunton, D. E., Cross, J. B., and Hakes, C. L., "EOIM-III Mass Spectrometry and Polymer Chemistry: STS 46. July–August 1992," *Journal of Spacecraft and Rockets*, Vol. 32, No. 3, 1995, pp. 483–495.

[9]Baird, J. K., "Low-Earth-Orbit Atomic Oxygen Erosion of Polymer Surfaces," *Journal of Spacecraft and Rockets*, Vol. 35, No. 1, 1998, pp. 62–65.

[10]DePristo, A. E., and Metiu, H., "Molecular Dynamics Simulations of Energy Flow at Solid Surface. New Methods Using a Small Number of Atoms," *Journal of Chemical Physics*, Vol. 90, No. 2, 1989, pp. 1229–1236.

[11]Lee, C.-H., and Chen, L. W., "Reactive Probability of Atomic Oxygen with Material Surfaces in Low Earth Orbit," *Journal of Spacecraft and Rockets*, Vol. 37, No. 2, 2000, pp. 252–256.

[12]Tenner, A. D., Sason, R. P., Gillen, K. T., Harrison, D. E., Horn, T. C. M., and Kleyn, A. W., "Computer Simulations and Rainbow Patterns of Alkali Ion Scattering from Metal Surface," *Surface Science*, Vol. 172, 1986, pp. 121–150.

[13]Valuev, A. A., Kakyyugin, A. S., and Norman, G. E., "Molecular Modeling of the Chemical Interaction of Atoms and Molecules with a Surface," *Russian Chemical Reviews*, Vol. 64, No. 7, 1995, pp. 599–625.

[14]Shustorovich, E., and Sellers, H., "The UBI-QEP Method: A Practical Theoretical Approach to Understanding Chemistry on Transition Metal Surfaces," *Surface Science Reports*, Vol. 31, 1998, pp. 1–119.

[15]Whitaker, A. F., and Jang, B. Z., "The Mass Loss Mechanisms of Polymers in a Radio Frequency Induced Atomic Oxygen Environment," *Journal of Applied Polymer Science*, Vol. 48, 1993, pp. 1341–1367.

[16]Tully, J. C., "Theories of the Dynamics of Inelastic and Reactive Processes at Surfaces," *Annual Review of Physics*, Vol. 31, 1980, pp. 319–343.

[17]Chen, L. W., and Lee, C.-H., "The Effective Attractive Potential in the Non-Retarded Regime for Molecules of Dielectric Materials via Lifshitz Theory," *Molecular Physics*, Vol. 99, No. 16, 2001, pp. 1381–1389.

[18]Ewig, C. S., Berry, R., Dinur, U., Hill, J.-R., Hwang, M.-J., Li, H. Y., Liang, C., Maple, J., Peng, Z. W., Stockfisch, T. P., Thacher, T. S., Yan, L., Ni, X. S., and Hagler, A. T., "Derivation of Class II Force Fields. VIII. Derivation of a General Quantum Mechanical Force Field for Organic Compounds," *Journal of Computational Chemistry*, Vol. 22, No. 15, 2001, pp. 1782–1800.

[19]Martinkevich, A. A., Prokopchuk, N. R., and Krotko, E. T., "The Influence of the Structure of the Dianhydride Fragment on Intermolecular Interactions in Linear Polyimides and Their Properties," *Polymer Degradation and Stability*, Vol. 66, No. 1, 1999, pp. 1–4.

[20]Mitra, S. S., "Debye Characteristic Temperature of Solids," *Journal of Scientific and Industrial Research*, Vol. 21A, 1962, pp.76–84.

[21]Mayne, H. R., "The Classical Trajectory Approach to Reaction Dynamics," *Dynamics of Molecules and Chemical Reactions*, edited by R. E. Wyatt and J. Z. H. Zhang, Dekker, New York, 1996, pp. 589–616.

[22]Raff, L. M., and Thompson, D. L., "The Classical Trajectory Approach to Reaction Scattering," *Theory of Chemical Reaction Dynamics*, edited by M. Baer, Vol. 3, CRC Press, Boca Raton, FL, 1985, pp. 1–121.

[23]Nørskov, J. K., "Chemisorption on the Metal Surfaces," *Reports on Progress in Physics*, Vol. 53, 1990, pp. 1253–1295.

[24]Wahnström, G., Lee, A. B., and Strömquist, J., "Motion of 'Hot' Oxygen Atom on Corrugated Metal Surfaces," *Journal of Chemical Physics*, Vol. 105, No. 1, 1996, pp. 326–336.

[25]Besenbacher, F., and Nørskov, J. K., "Oxygen Chemisorption on Metal Surfaces: General Trends for Cu, Ni and Ag," *Progress in Surface Science*, Vol. 44, 1993, pp. 5–66.

[26]Gelb, A., Sumpter, B. G., and Noid, D. W., "Computer Simulation of Molecular Collision with a Polymer Surface," *Journal of Physical Chemistry*, Vol. 94, No. 2, 1990, pp. 809–814.

[27]Goodman, F. O., and Wachman, H. Y., *Dynamics of Gas-Surface Scattering*, Academic Press, New York, 1976, pp. 255–314.

[28]Verlet, L., "Computer 'Experiments' on Classical Fluids. I. Thermodynamical Properties of Lennard–Jones Molecules," *Physical Reviews*, Vol. 159, No. 1, 1967, pp. 98–103.

[29]Baklagina, Yu. G., and Milevkaya, I. S., "Supermolecular Structure of Polyamic Acids and Polymides," *Polyamic Acids and Polyimides: Synthesis, Transformations, and Structure*, edited by M. I. Bessonov and V. A. Zubkov, CRC Press, Boca Raton, FL, 1993, Chap. 4.

[30]Leach, A. R., *Molecular Modelling: Principles and Applications*, Addison Wesley Longman, Beijing, 1996, Chap. 3.

[31]Scialdone, J. J., Clatterbuck, C. H., Ayres-Treusdell, M., Park, G., and Kolos, D., "Evaluation of Certain Material Films Flown on the Space Shuttle Mission 46, EOIM III Experiment," NASA TM-104621, Sept. 1995.

[32]Reddy, M. R., Srinivasamurthy, N., and Agrawal, B. L., "Effect of the Low-Earth-Orbit Atomic-Oxygen Environment on Solar-Array Materials," *ESA Journal*, Vol. 16, 1992, pp. 193–208.

[33]Brinza, D. E., Chung, S. Y., Minton, T. K., and Liang, R. H., "Final Report on the NASA/JPL Evaluation of Oxygen Interactions with Materials—3 (EOIM—3)," NASA CR-198865, Dec. 1994.

[34]Krech, R. H., Gauthier, M. J., and Caledonia, G. E., "High Velocity Atomic Oxygen/Surface Accommodation Studies," *Journal of Spacecraft and Rockets*, Vol. 30, No. 4, 1993, pp. 509–513.

[35]Zhang, Jianming, Garton, D. J., and Minton, T. K., "Reactive and Inelastic Scattering Dynamics of Hyperthermal Oxygen Atoms on a Saturated Hydrocarbon Surface," *Journal of Chemical Physics*, Vol. 117, No. 13, 2002, pp. 6239–6251.

[36]Visentine, J. T., Leger, L. J., Kuminecz, J. F., and Spiker, I. K., "STS-8 Atomic Oxygen Effects Experiment," AIAA 85-0415, Jan. 1985.

[37]Yokota, K., Tagawa, M., and Ohmae, N., "Impingement Angle Dependence of Erosion Rate of Polyimide in Atomic Oxygen Exposures," *Journal of Spacecraft and Rockets*, Vol. 39, No. 1, 2002, pp. 155, 156.

[38]Koontz, S. L., Albyn, K., and Leger, L. J., "Atomic Oxygen Testing with Thermal Atom System: A Critical Evaluation," *Journal of Spacecraft and Rockets*, Vol. 28, No. 3, 1991, pp. 315–323.

[39]Grossman, E., and Lifshitz, Y., "In Situ Erosion Study of Kapton Using Novel Hyperthermal Oxygen Atom Source," *Journal of Spacecraft and Rockets*, Vol. 36, No. 1, 1999, pp. 75–78.

[40]Skurat, V. E., "Probability Estimation of the Chemical Reaction upon Collisions of Oxygen Atoms of the Energy 5 eV with the Surfaces of Various Organic Polymers," *Doklady Physical Chemistry*, Vol. 349, Nos. 1–3, 1996, pp. 159–162.

[41]Hoffmann, R., *Solid and Surface: A Chemist's View of Bonding in Extended Structures*, VCH, New York, 1988.

[42]Grimley, T. B., "Gas–Surface Interactions: Basic Thermodynamics and Recent Work on Sticking," *Interaction of Atoms and Molecules with Solid Surface*, edited by V. Bortolani, N. H. March, and M. P. Tosi, Plenum, New York, 1990, Chap. 3.

[43]Pauling, L., *The Nature of the Chemical Bond*, 3rd ed., Cornell Univ. Press, Ithaca, NY, 1960, Chap. 7.

[44]Pearson, R. G., "Absolution Electronegativity and Absolute Hardness," *Theoretical Models of Chemical Bonding, Vol. 2, The Concept of the Chemical Bond*, edited by Z. B. Maksić, Springer-Verlag, Berlin, 1990, pp. 45–76.

[45]Kafafi, S. A., LaFemina, J. P., and Nauss, J. L., "Electronic Structure and Conformation of Polymers from Cluster Molecular Orbital and Molecular Mechanics Calculations: Polyimide," *Journal of the American Chemical Society*, Vol. 112, No. 24, 1990, pp. 8742–8746.

[46]Lide, D. R. (ed.), "Molecular Structure and Spectroscopy," *CRC Handbook of Chemistry and Physics*, 82nd ed., CRC Press, Boca Raton, FL, 2001, pp. 9.1–9.96.

[47]Pauling, L., "The Nature of the Chemical Bond. IV. The Energy of Single Bonds and the Relative Electronegativity of Atoms," *Journal of the American Chemical Society*, Vol. 54, No. 9, 1932, pp. 3570–3582.

[48]Schomker, V., and Stevenson, D. P., "Some Revisions of the Covalent Radii and the Additivity Rule for the Lengths of Partially Ionic Single Covalent Bonds," *Journal of the American Chemical Society*, Vol. 63, No. 1, 1941, pp. 37–40.

[49]Polansky, O. E., and Derflinger, G., "Über den Zusammenhang von Bindungslängen und Elektronegativitäten," *Thermochimica Acta*, Vol. 1, 1963, pp. 308–326.

[50]Mönch, W., *Semicondutor Surfaces and Interfaces*, Springer-Verlag, New York, 1993, Chap. 3.

[51]Bergmann, D., and Hinze, J., "Electronegativity and Charge Distribution," *Electronagativity*, edited by K. D. Sen and C. K. Jørgensen, Springer-Verlag, Berlin, 1987, pp. 145–190.

[52]Bessonov, M. I., Koton, M. M., Kudryavtsev, V. V., and Laius, L.A., *Polyimides: Thermally Stable Polymers*, Consultants Bureau, New York, 1987.

[53]Ghosh, M. K. (ed.), *Polyimides: Fundamentals and Applications*, Dekker, New York, 1996, p. 787.

[54]Anderson, O. L., "A Simple Method for Calculating the Debye Temperature from Elastic Constants," *Journal of Physics and Chemistry of Solids*, Vol. 24, 1963, pp. 909–917.

[55]Debye, P., "X-Ray Interference and Thermal Movement," *The Collected Papers of J. W. Debye*, Interscience, New York, 1954, pp. 3–39.

[56]Cho, S. H., Kim, G., McCarthy, T. J., and Farris, R. J., "Orthotropic Elastic Constants for Polyimide Film," *Polymer Engineering and Science*, Vol. 41, No. 2, 2001, pp. 301–307.

[57]Huntington, H. R., "The Elastic Constants of Crystals," *Solid State Physics*, edited by F. Seitz and D. Turnbull, Vol. 7, Academic Press, New York, 1958, pp. 214–351.

D. Edwards
Associate Editor